# COEXISTENCE OF REGIONS OF EQUILIBRIUM AND NON-EQUILIBRIUM TWO-POINT TURBULENCE DYNAMICS IN GRID-GENERATED TURBULENCE BOTH WITH $-5/3$ SPECTRA BUT DIFFERENT UNDERLYING PHYSICS

**Sylvain Laizet**
Turbulence, Mixing and Flow Control Group,
Department of Aeronautics, Imperial College London
London, SW7 2AZ, United Kingdom
s.laizet@imperial.ac.uk

**J.Christos Vassilicos**
Turbulence, Mixing and Flow Control Group,
Department of Aeronautics, Imperial College London
London, SW7 2AZ, United Kingdom
j.c.vassilicos@imperial.ac.uk

## ABSTRACT

In this paper we present results concerning the spatial development of energy spectra $E_{11}(f)$ and their associated integral and Taylor scales in conjunction with the spatial developments of vorticity, strain and production rates of vorticity and strain obtained from Direct Numerical Simulations of spatially developing grid-generated turbulence. We use a fractal square grid and a single mesh grid where the mesh is similar to the largest square on the fractal square grid.

We find two adjacent but physically different regions in these flows relatively close to the grid: one where the *Q*-*R* diagram has not yet formed its well-known, presumed universal, tear-drop shape Tsinober (2009) but $E_{11}(f) \sim f^{-5/3}$ over more than a decade of a frequency range which is set by inlet conditions rather than Kolmogorov scalings: and one where the *Q*-*R* diagram immediately adopts the well-known tear-drop shape and $E_{11}(f) \sim f^{-5/3}$ over a Kolmogorov range of frequencies which increases as the local Reynolds number increases. In the one case where the local Reynolds number is high enough, the first region gives rise, as one moves downstream, to the non-equilibrium behaviour $C_\varepsilon \sim 1/Re_\lambda$ whilst the second region leads to $C_\varepsilon = Const$.

## INTRODUCTION

Recent wind tunnel and water channel experiments by Seoud & Vassilicos (2007); Mazellier & Vassilicos (2010); Valente & Vassilicos (2011, 2012); Gomes-Fernandes *et al.* (2012); Discetti *et al.* (2013); Nagata *et al.* (2013) have revealed that a substantial region of well-developed decaying turbulence exists in the lee of space-filling fractal square and regular grids where the ratio of the integral length-scale $L$ to the Taylor microscale $\lambda$ remains approximately constant as the turbulence and the Reynolds number $Re_\lambda \equiv \frac{u'\lambda}{\nu}$ decay ($u'^2$ is a measure of the turbulent kinetic energy and $\nu$ is the kinematic viscosity). The direct implication is that the normalised dissipation constant $C_\varepsilon$ scales as $C_\varepsilon \sim 1/Re_\lambda$ in that region, in stark contrast with the assumption $C_\varepsilon = Const$ refered to by Tennekes & Lumley Tennekes & Lumley (1972) as "one of the cornerstone assumptions of turbulence theory". This is a region of well-developed turbulence in the sense that the statistics of turbulent fluctuating velocities are approximately gaussian and Eulerian energy spectra have well-defined power-law shapes with exponents close to $-5/3$ over at least one decade of wavenumbers (see references mentioned above). This is also a region where the turbulence can be considered to be out of two-point equilibrium because the normalised rate of interscale energy transfer can be expected to be constant over a significant range of scales and therefore out of balance with the normalised dissipation rate $C_\varepsilon \sim 1/Re_\lambda$ during streamwise decay.

In this paper we investigate grid-generated turbulence numerically and include in our investigation the production region upstream of the decay region where the new non-equilibrium dissipation law has been observed Seoud & Vassilicos (2007); Mazellier & Vassilicos (2010); Valente & Vassilicos (2011, 2012); Gomes-Fernandes *et al.* (2012); Discetti *et al.* (2013); Nagata *et al.* (2013). An important question which arises from these experimental studies has to do with the presence of the well-defined $-5/3$ power law energy spectrum in the non-equilibrium decay region even though such spectra are usually derived for and explained to be the consequence of equilibirum Richardson-Kolmogorov cascade dynamics Batchelor (1953). Could it be that $-5/3$ spectra appear already in the production region as a result of very different dynamics? Would such dynamics, if they exist, be also responsible for the new dissipation law further downstream or are the two phenomena unrelated?

Universality properties have been claimed for energy spectra, for the well-known *Q*-*R* diagram and for aspects of strain rate production and vortex stretching. All these properties have been related to the turbulence cascade pro-

cess (read Tsinober (2009) for a critical discussion). We therefore address the questions posed in the previous paragraph by concurrent calculations of energy spectra on the one hand and vorticity, strain and their production rates on the other. This post-processing is applied on data obtained from Direct Numerical Simulations (DNS) of spatially developing grid-generated turbulence. We use a fractal square grid (see figure 1) and a single mesh grid where the mesh is similar to the largest square on the fractal square grid.

## METHODOLOGY

We assume a fluid of uniform density and kinematic viscosity $\nu$ and inflow/outflow boundary conditions in the streamwise direction with a uniform fluid velocity $U_\infty$ (without turbulence) as inflow condition and a 1D convection equation as outflow condition. The boundary conditions in the two spanwise directions are periodic. In terms of the lateral thickness $D$ of the largest bars on the grids, the inlet Reynolds number $Re_D \equiv \frac{U_\infty D}{\nu}$ is 2550 for the fractal square grid of figure 1 and 4320 for the case of a grid made of only one square mesh corresponding to the biggest square of the fractal square grid in figure 1 (but with bar thickness $D$ that is about 1.7 times larger). Our initial condition for the velocity field is $\mathbf{u} \equiv (u,v,w) = (U_\infty, 0, 0)$ everywhere ($u$ is the streamwise velocity component and $(v,w)$ are the two spanwise velocity components corresponding to spatial spanwise coordinates $(y,z)$).

Each grid is placed in a computational domain with streamwise length $L_x$ and spanwise extents $L_y = L_z = T$. For the fractal square grid, $L_x = 8T = 144D$ and for the single square grid $L_x = 4T = 40D$. Defining $x$ to be the spatial coordinate in the streamwise direction and the grids to be at $x = 0$, the inflow is at $x = -10D$ for the fractal square grid and at $x = -6.5D$ for the single square. The streamwise thickness of both turbulence generators is $3t_{min}$ where $t_{min}$ is the spanwise thickness of the smallest bars on the fractal square grid. The centres of both grids coincide with the centreline of the domain.

We solve the incompressible Navier-Stokes equations on a Cartesian mesh with the numerical code **Incompact3d** which is based on sixth-order compact schemes for spatial discretization and a third order Adams-Bashforth scheme for time advancement. To treat the incompressibility condition, a fractional step method requires to solve a Poisson equation. This equation is fully solved in spectral space, via the use of relevant 3D Fast Fourier Transforms. The pressure mesh is staggered from the velocity mesh by half a mesh, to avoid spurious pressure oscillations. With the help of the concept of modified wave number, the divergence-free condition is ensured up to machine accuracy. The modelling of the grids is performed by an Immersed Boundary Method, following a procedure proposed by Parnaudeau *et al.* (2008). The present method is a direct forcing approach that ensures the no-slip boundary condition at the grid walls. It mimics the effects of a solid surface on the fluid with an extra forcing in the Navier-Stokes equations. Full details about the code, its validations and its application to grid-generated turbulence can be found in Laizet & Lamballais (2009); Laizet & Vassilicos (2011).

Because of the size of the simulations, the parallel version of **Incompact3d** has been used for this numerical work. Based on a highly scalable 2D decomposition library and a distributed FFT interface, it is possible to use the code on thousands of computational cores. More details about this efficient parallel strategy can be found in Laizet & Li (2011).

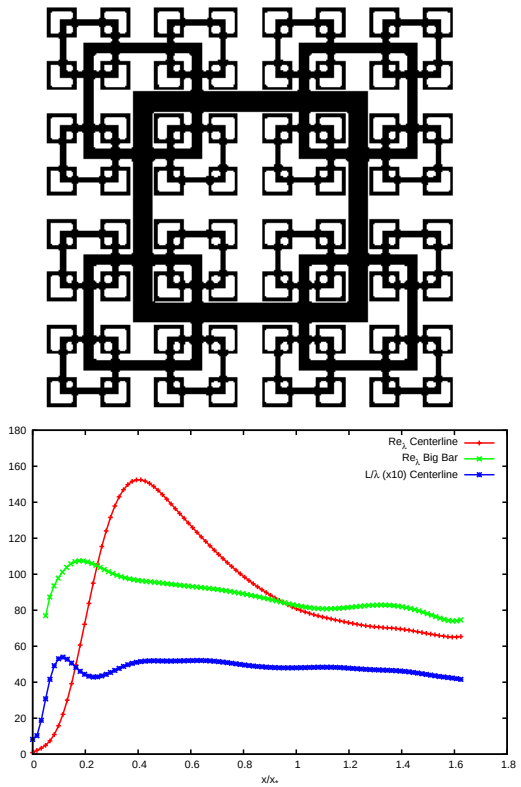


Figure 1. Fractal square grid and streamwise plots of $10L/\lambda$ along centreline and $Re_\lambda$ along centreline and line crossing a big bar at the middle. Fractal grid case.

For the turbulent flow generated by the fractal square grid in figure 1, the Cartesian mesh has 2881 nodes in the streamwise direction and $360 \times 360$ nodes in the other two directions. For the case of the grid made of only one square, the Cartesian mesh has 1441 nodes in the streamwise direction and $360 \times 360$ nodes in the other two directions. The time step is $\Delta t = 0.01 t_{min}/U_\infty$ in both simulations and the spatial resolution is one to two Kolmogorov length-scales $\eta$ in the vast majority of the computational domain. Our DNS can therefore be considered to be reasonably well resolved.

Statistics are collected and averages taken over $10^6$ time steps at various points in the flow along the centreline normal to either grid; and along a line normal to either grid and crossing the big or biggest bar at the middle.

### Parametric description of the turbulence generators

The fractal grid that we use is a space-filling fractal square grid (see Hurst & Vassilicos (2007) where full details on the design of such grids can be found). Our fractal square grid has $N = 4$ iterations (using the definition of $N$ given in Hurst & Vassilicos (2007)). The first iteration $j = 0$ is made of a single square which consists of four bars each of length $L_0$ and lateral thickness $t_0 = D$. The subsequent iterations $j = 2, 3, 4$ have $4^{j-1}$ scaled-down squares made of bars of length $L_j = R_L^j L_0$ and lateral thicknesses $t_j = R_t^j t_0$ (in the plane of the grid, normal to the mean flow) where $R_L = 1/2$, $L_0 = 0.5 L_y$. By definition, $L_0 = L_{max}$, $L_{N-1} = L_{min}$, $t_0 = t_{max}$ and $t_{N-1} = t_{min}$. The thickness ratio $t_r \equiv t_{max}/t_{min}$, i.e. the ratio between the lateral thicknesses of the

| | $n_x \times n_y \times n_z$ | $L_x \times L_y \times L_z$ ($t_{min}$) | Grid | $\sigma$ | $t_0 = D$ |
|---|---|---|---|---|---|
| DNS1 | 2881×360×360 | 1152×144×144 | $fractal\square$ | 0.5 | $8.5t_{min}$ |
| DNS2 | 1441×360×360 | 576×144×144 | Single mesh | 0.16 | $14.4t_{min}$ |

Table 1. Numerical parameters of the simulations and characteristics of the two grids.

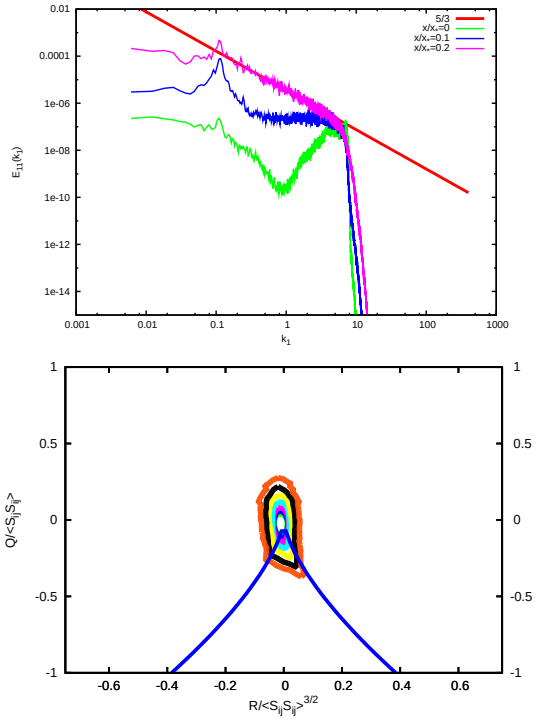


Figure 2. Energy spectra at different $x/x_* = 0, 0.1, 0.2$ (the straight line has a $-5/3$ slope for reference). $Q$-$R$ diagram at $x/x_* = 0.2$. Centreline, fractal grid.

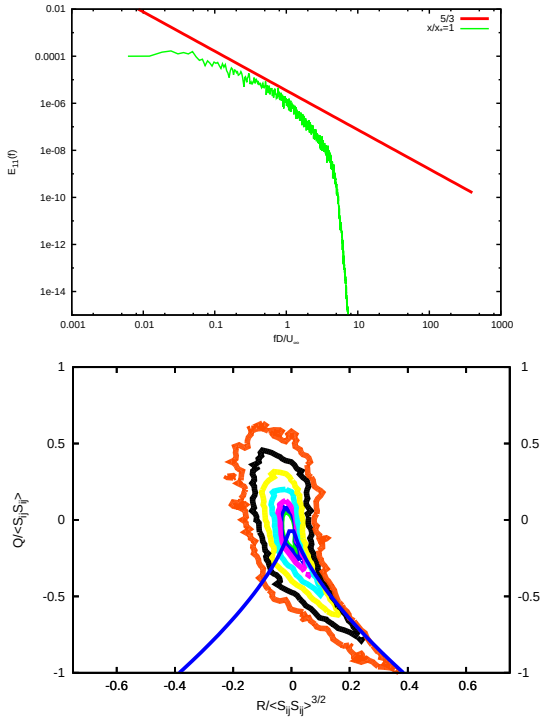


Figure 3. Energy spectrum and $Q$-$R$ diagram at $x/x_* = 1$ (the straight line in the spectral plot has a $-5/3$ slope for reference). Centreline, fractal grid.

largest to the smallest bars, is $t_r = 8.5$ (the value of $t_r$ can be used to derive $R_t$). The blockage ratio $\sigma$ of our fractal grid, defined as the ratio of its total lateral area to $T^2 = L_y \times L_z$, is $\sigma = 50\%$. The other grid has $\sigma = 16\%$. See Table 1 for a summary.

## RESULTS

Figure 1 shows, as functions of $x/x_*$ (where $x_*$ is the wake-interaction length-scale defined for grid-generated turbulence by Mazellier & Vassilicos (2010), but see also Gomes-Fernandes *et al.* (2012)), $L/\lambda$ and $Re_\lambda$ along the centreline for the fractal grid case and $Re_\lambda$ along a line crossing at the middle of a biggest bar on the fractal grid. The significance of $x_*$ is that the position $x_{peak}$ of the turbulence peak scales with it along the centreline. The centreline peak in $Re_\lambda$ is at $x_{peak} \approx 0.4x_*$ in figure 1 in approximate agreement with laboratory experiments Mazellier & Vassilicos (2010); Gomes-Fernandes *et al.* (2012); Discetti *et al.* (2013).

At $x/x_* < 0.4$ the turbulence fluctuating velocities are known to be non-gaussian but they are also known to be gaussian at $x/x_* > 0.4$ Mazellier & Vassilicos (2010). We see clearly in figure 2 the result previously reported from the laboratory experiments of Seoud & Vassilicos (2007); Mazellier & Vassilicos (2010); Valente & Vassilicos (2011, 2012); Gomes-Fernandes *et al.* (2012); Discetti *et al.* (2013) that, in the decay region $x/x_* > 0.4$, $L/\lambda$ remains approximately constant as $Re_\lambda$ decays along the centreline: i.e. as the local Reynolds number decreases, the range of excited length-scales in the turbulence spectrum remains about the same. This behaviour does not tie up easily with usual Richardson-Kolmogorov cascade phenomenology and implies, in particular, an unusual behaviour for the dissipation rate which is determined by the turbulent strain rate field.

The study of the turbulent strain rate field $s_{ij}$ closely involves the turbulence fluctuating vorticity $\omega_i$. One way to obtain some insight into their statistics is in terms of the $Q$-$R$ diagram Tsinober (2009) where $Q \equiv \frac{1}{4}(\omega_i\omega_i - 2s_{ij}s_{ij})$ and $R \equiv -\frac{1}{3}(s_{ij}s_{jk}s_{ki} + \frac{3}{4}\omega_i s_{ij}\omega_j)$. All data to this day (see Tsinober (2009)) indicate that this diagram has the tear drop shape shown in figures 3 and 4 in many turbulent flows. This is indeed the case in our flows either far enough downstream along the centreline ($x/x_* = 1$ in figure 3) or all along a streamwise line crossing the largest bar at the middle (see figure 4). However, at distances from the grid which are smaller than about $x_{peak}$ the tear drop shape is not so clearly defined. This is particularly significant because, as shown in figure 2, the energy spectrum develops a $-5/3$ power-law shape in exactly such a region (around

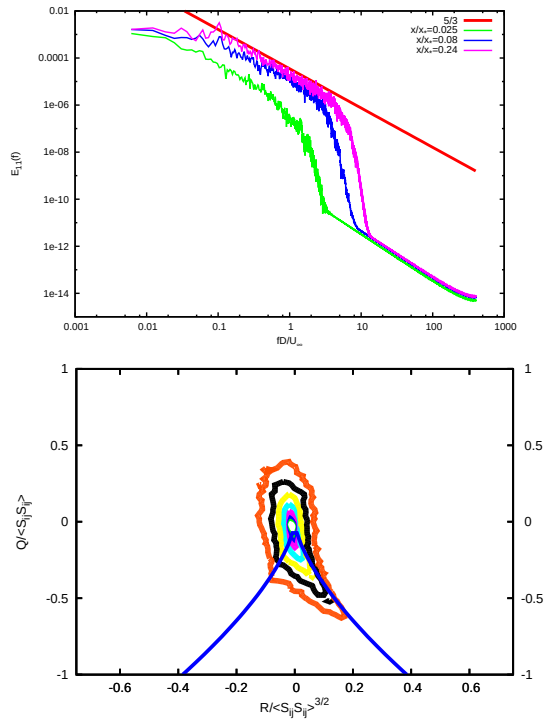


Figure 4. Energy spectra at different $x/x_* = 0.025, 0.08, 0.24$ (the straight line has a $-5/3$ slope for reference). *Q-R* diagram at $x/x_* = 0.025$. Data along line crossing big bar of single square grid.

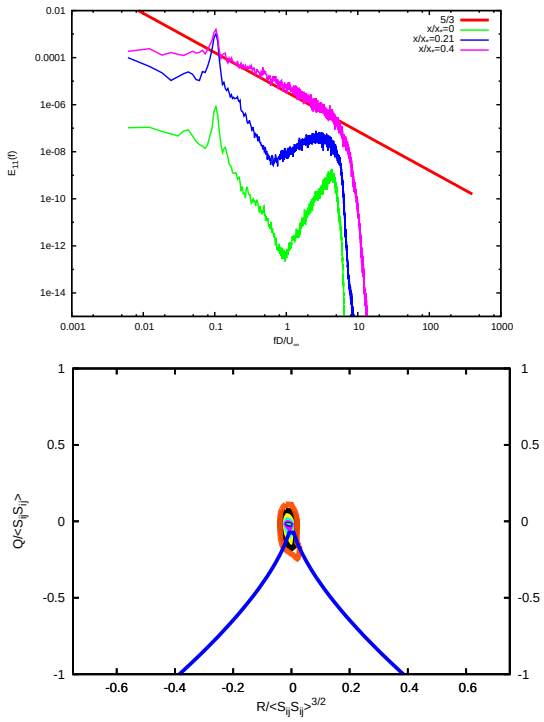


Figure 5. Energy spectra at different $x/x_* = 0, 0.21, 0.4$ (the straight line has a $-5/3$ slope for reference). *Q-R* diagram at $x/x_* = 0.4$. Data along centerline of single square grid.

$x/x_* = 0.2$ in the case of the fractal grid). This also happens to be a region of highly non-gaussian, i.e. very intermittent, fluctuating velocities. Further downstream along the centreline, the energy spectrum loses its power law shape as the local Reynolds number decays but the flow acquires the well-known *Q-R* tear-drop shape (see Figure 3). The results described in this paragraph hold for both turbulence generators, the main differences being the normalised peak distance $x_{peak}/x_*$ and the normalised distance $x/x_*$ where the $-5/3$ spectrum appears along the centreline; both these two normalised distances are smaller for the fractal square grid (see figures 5 and 6 for results equivalent to those of figures 2 and 3 but for the single square grid).

Along a streamwise line in a neighboring region dominated by the wake of the big bar the *Q-R* diagram adopts a clear tear-drop shape over the usual quantitative extent (see figure 4) from the outset and keeps it throughout this line in our computations. The energy spectrum emerges with a broad range of excited power-law scales from the outset too (very small $x/x_*$, see figure 4) but evolves towards a $-5/3$ spectrum over an increasing range of scales as it spatially develops downstream. This increase in the range of scales is brought about by the decrease of the Kolmogorov microscale with distance from the grid owing to the increasing local Reynolds number.

Note that the $-5/3$ range is set in a very different way in the centreline region. Very close to the grid along the centreline, the energy spectrum is dominated by two excited frequencies, one being the shedding frequency of the big bar wakes and the other characterising the secondary instability of the shear-layersDong *et al.* (2006). These frequencies differ by a factor of about 40 in both our flows. The range over which the $-5/3$ spectrum develops is determined by

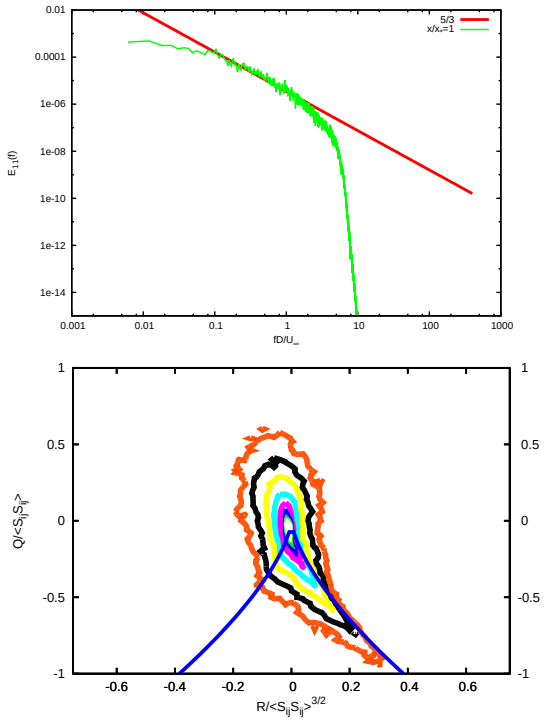


Figure 6. Energy spectrum and *Q-R* diagram at $x/x_* = 1$ (the straight line in the spectral plot has a $-5/3$ slope for reference). Centreline, single square grid.

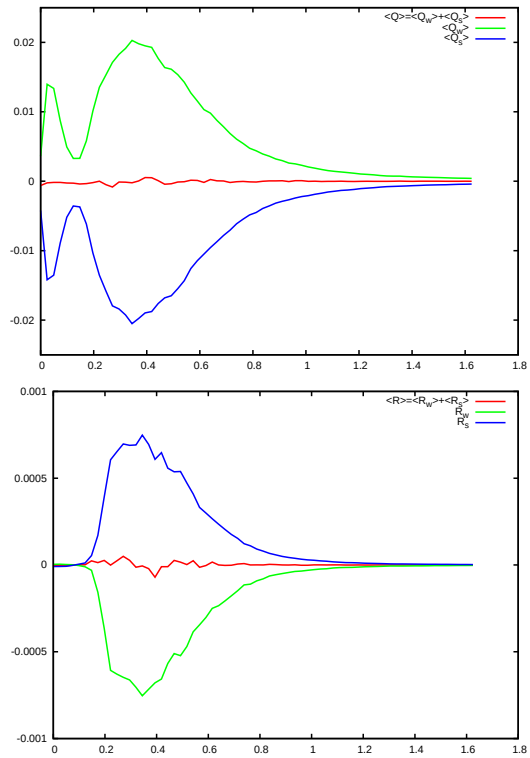


Figure 7. Plots of $Q_w$, $Q_s$ and $Q$ on the left and of $R_w$, $R_s$ and $R$ on the right as functions of $x/x_*$. Centreline of the fractal square grid.

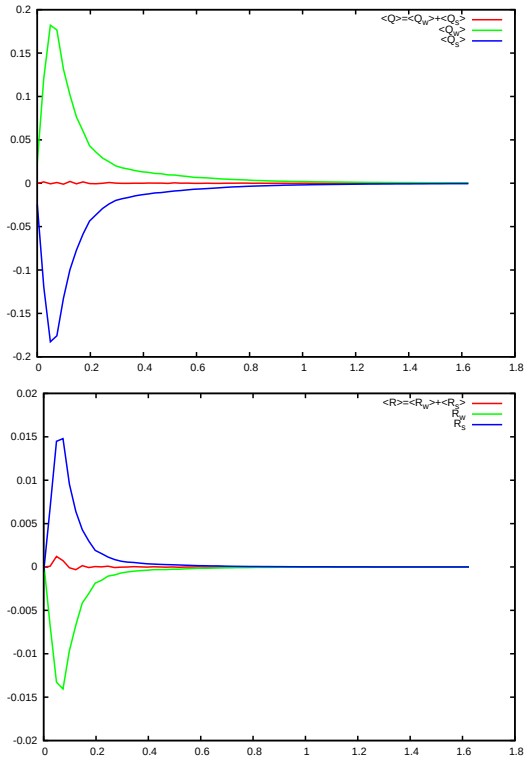


Figure 8. Plots of $Q_w$, $Q_s$ and $Q$ on the left and of $R_w$, $R_s$ and $R$ on the right as functions of $x/x_*$ along the streamwise straight line which crosses one of the largest bars of the fractal square grid in the middle.

these two frequencies and its extent is given by their ratio 40. Furthermore the local $Re_\lambda$ at the location where the $-5/3$ power-law first appears ($x/x_* \approx 0.2$ in the case of the fractal grid) is no more than about 60 (see figure 1), way too small for such a well-defined -5/3 power law over more than a decade (see figure 2). This is therefore a spectrum where the range of length-scales is directly set by inlet conditions and does not obviously relate to Kolmogorov scalings or local Reynolds number values.

Important differences in interscale and velocity gradient dynamics as sampled along the centreline on the one hand or the streamwise line dominated by the big bar on the other can also be seen in the streamwise developments of the rates of mean enstrophy and strain rate production.

Defining $Q_w \equiv \frac{1}{4}\omega^2$, $Q_s \equiv -\frac{1}{2}s_{ij}s_{ij}$, $R_w \equiv -\frac{1}{4}\omega_i\omega_j s_{ij}$ and $R_s \equiv -\frac{1}{3}s_{ij}s_{jk}s_{ki}$, in figure 7 we plot $< Q_w >$, $< Q_s >$ and $< Q >=< Q_w + Q_s >$ as functions of $x/x_*$ as well as $< R_w >$, $< R_s >$ and $< R >=< R_w + R_s >$ as functions of $x/x_*$ along the centerline for the fractal grid (similar results are obtained for the single square grid and a similar discussion can be made). Firstly we note that $< Q >= 0$ and $< R >= 0$ throughout the domain along the centerline. This is not a trivial result because our turbulent flows are not homogeneous, particularly at $x < x_*$ (see Seoud & Vassilicos (2007); Mazellier & Vassilicos (2010); Laizet & Vassilicos (2011); Valente & Vassilicos (2011)). Secondly, we note the remarkable region $0 < x/x_* < 0.16$ along the centreline where $< R_w >=< R_s >= 0$ but $< Q_w >$ and $< Q_s >$ are not zero. Then something happens around $x/x_* \approx 0.16$ which sets off non-zero values of average enstrophy and strain rate production rates. This is also about where the energy spectrum adopts its well-defined $-5/3$ power-law shape over more than one decade (see figure 2). At this point, $< R_w >$ and $< R_s >$ start growing in magnitude (with opposite signs to keep $< R >= 0$) and reach a peak where the local Reynolds number peaks (see figure 1). $< Q_w >$ and $< Q_s >$ peak at the same point. Further downstream, $< R_w >$, $< R_s >$, $< Q_w >$, $< Q_s >$ and $Re_\lambda$ continuously decay together.

The negative sign of $< R_w >$ throughout the region where it is non-zero implies positive enstrophy production which would imply a creation of increasingly small-scales (perhaps a cascade of sorts) in the sense that fluctuating velocity derivatives on average increase. No such behaviour seems to exist in the region $0 < x/x_* < 0.16$ along the centreline where the energy spectrum progressively develops towards the best defined $-5/3$ power-law over the widest range in the entire flow domain (see figure 2). The increase and then decrease of enstrophy along the centerline in this region may have to do with enstrophy being advected from nearby then left to decay as it is swept downstream for as long as enstrophy production has not yet started.

The situation is very different in the lee of one of the largest bars of the grid as can be seen in figure 8 where $Q_w$, $Q_s$ and $Q$ and $R_w$, $R_s$ and $R$ are plotted as in figure 7 but along the streamwise straight line which crosses one of the largest bars of the fractal square grid in the middle. This is a region dominated by the planar wake of one of the biggest bars (we present the plots obtained for the fractal grid but similar results are obtained for the single square grid and a similar discussion can be made). In stark contrast with the behviour along the centreline, average enstrophy and strain rate production rates start building up immediately after the bar and so does the power-law energy spectrum which seems to develop in a more usual Richardson-Kolmogorov fashion as Reynolds number increases (see figure 4 and keep in mind that a similar figure can be provided

for the fractal square grid). Similarly to figure 7, though, $< Q >= 0$ and $< R >= 0$ throughout the domain along the streamwise line inside the planar wake of a largest bar.

## CONCLUSION

Our simulations have revealed the coexistence side by side of two very different mechanisms for the generation of $-5/3$ energy spectra. One appears to be based on strain rate and enstrophy production and a cascade which has attributes similar to that of a Richardson-Kolmogorov phenomenology. The other is very different and appears less reliant on local Reynolds number and strain rate and enstropy production, however much more dependent on initial conditions and global Reynolds number. The initial conditions impact via the properties, e.g. frequencies, of vortex shedding and secondary instabilities and may therefore have different effects at different Reynolds number. It will be important to extend the present study to similar but higher Reynolds number flows.

It is unclear whether the centreline mechanism for generating a non-Kologorov $-5/3$ energy spectrum is also responsible for the new non-equilibrium dissipation law recently discovered in wind tunnel and water channel experiments Seoud & Vassilicos (2007); Mazellier & Vassilicos (2010); Valente & Vassilicos (2011, 2012); Gomes-Fernandes *et al.* (2012); Discetti *et al.* (2013); Nagata *et al.* (2013). In the case of the single square grid we do not observe this new dissipation law in the present simulations but a similar grid to our single square grid does return this law in the decaying region of the wind tunnel experiment of Valente & Vassilicos (2012). However, the Reynolds number in this wind tunnel experiment is much larger than here and this could be a factor to take into account. The cross-over Reynolds number value for the new dissipation law to be possible may well depend on the type of grid and may, in fact, be lower for the present fractal square grid than for the present single squre grid.


## Acknowledgements

The authors are grateful to Dr. Ning Li for helping with the parallel version of **Incompact3d**. We also thank Eric Lamballais for very useful discussions and acknowledge support from EPSRC Research grants EP/E00847X/1 and EP/F051468/1.


## REFERENCES


Batchelor, G.K. 1953 *The theory of homogeneous turbulence*. Cambridge University Press.

Discetti, S., Ziskin, I. B., Astarita, T. & Adrian, R. J. 2013 Piv measurements of anisotropy and inhomogeneity in decaying fractal generated turbulence. *Fluid Dynamics Research* **submitted**.

Dong, S., Karniadakis, G.E., Ekmekci, A. & Rockwell, D. 2006 A combined direct numerical simulation-particle image velocimetry study of the turbulent near wake. *J. Fluid Mech.* **569**, 185–207.

Gomes-Fernandes, R., Ganapathisubramani, B. & Vassilicos, J. C. 2012 PIV study of fractal-generated turbulence. *J. Fluid Mech.* **701**, 306–336.

Hurst, D. & Vassilicos, J. C. 2007 Scalings and decay of fractal-generated turbulence. *Phys. Fluids* **19** (035103).

Laizet, S. & Lamballais, E. 2009 High-order compact schemes for incompressible flows: a simple and efficient method with the quasi-spectral accuracy. *J. Comp. Phys.* **228(16)**, 5989–6015.

Laizet, S. & Li, N. 2011 Incompact3d, a powerful tool to tackle turbulence problems with up to $o(10^5)$ computational cores. *Int. J. Numer. Methods Fluids* **67(11)**, 1735–1757.

Laizet, S. & Vassilicos, J. C. 2011 Dns of fractal-generated turbulence. *Flow, Turbulence and Combustion* **87(4)**, 673–705.

Mazellier, N. & Vassilicos, J. C. 2010 Turbulence without Richardson-Kolmogorov cascade. *Phys. Fluids* **22** (075101).

Nagata, K., Sakai, Y., Suzuki, H., Suzuki, H., Terashima, O. & Inaba, T. 2013 Turbulence structure and turbulence kinetic energy transport in multiscale/fractal-generated turbulence. *Phys. Fluids* p. Submitted to.

Parnaudeau, P., Carlier, J., Heitz, D. & Lamballais, E. 2008 Experimental and numerical studies of the flow over a circular cylinder at Reynolds number 3900. *Phys. Fluids* **20**, 085101.

Seoud, R. E. & Vassilicos, J. C. 2007 Dissipation and decay of fractal-generated turbulence. *Phys. Fluids* **19** (105108).

Tennekes, H. & Lumley, J. L. 1972 *A first course in turbulence*. MIT Press, Cambridge, Mass.

Tsinober, A. 2009 *An informal conceptual introduction to turbulence*. Springer.

Valente, P. & Vassilicos, J. C. 2011 The decay of turbulence generated by a class of multi-scale grids. *J. Fluid Mech.* **687**, 300–340.

Valente, P. & Vassilicos, J. C. 2012 Universal dissipation scaling for non-equilibrium turbulence. *Phys. Rev. Lett.* **108**, 214503.